JGR Earth Surface

RESEARCH ARTICLE
10.1029/2021JF006454

Evidence of Seasonal Uplift in the Argentière Glacier (Mont Blanc Area, France)

Christian Vincent[1], Adrien Gilbert[1], Andrea Walpersdorf[2], Florent Gimbert[1], Olivier Gagliardini[1], Bruno Jourdain[1], Juan Pedro Roldan Blasco[1], Olivier Laarman[1], Luc Piard[1], Delphine Six[1], Luc Moreau[3], Diego Cusicanqui[1], and Emmanuel Thibert[4]

[1]Université Grenoble Alpes, CNRS, IRD, Grenoble-INP, Institut des Géosciences de l'Environnement (IGE, UMR 5001), Grenoble, France, [2]Université Grenoble Alpes, CNRS, ISTerre, Grenoble, France, [3]Chamonix Glaciologie Association, Chamonix, France, [4]Université Grenoble Alpes, INRAE, UR ETGR, Grenoble, France

Abstract The hydromechanical processes by which basal water controls sliding at the glacier bed are poorly known, despite glacier basal motion being responsible for a large part of ice flux in temperate alpine glaciers. Previous studies suggest that sliding strongly relates to the quantity of water being stored at the ice-bedrock interface. However, this water storage is difficult to quantify accurately on the basis of surface-motion observations, given that uplift can also be affected by changes in vertical-strain rates and sliding velocity change. Here, we use a comprehensive data set of *in situ* measurements performed over 2 years on the Argentière Glacier in the French Alps to investigate the relationships between horizontal and vertical velocities, basal sliding, subglacial runoff and bed separation. We observe strikingly large uplifts varying spatially between 0.20 and 0.90 m over the winter/spring seasons between January and June and with a consistent spatial pattern from 1 year to another. We show, based on observations and three dimensional ice-flow modeling, that these large uplifts cannot be explained solely by changes in strain rates or in sliding up an inclined bed. Our results reveal that more than 80% of the observed uplift is related to enhanced bed separation through cavitation, allowing us to estimate the volume occupied by water-filled subglacial cavities. Our interpretation of uplift being mainly caused by increased cavitation is also consistent with an associated increase in the observed surface horizontal velocity. These findings provide important observational constraints for testing subglacial hydrological models.

Plain Language Summary Glacier basal motion is responsible for a large part of ice flux in temperate alpine glaciers and outlet glaciers of ice sheets. However, the hydromechanical processes by which basal water controls sliding at the glacier bed are poorly known in large part because observations are very scarce. Consequently, the impact of surface melting and meltwater input on the future of mountain glaciers and outlet glaciers of ice sheets remains unclear. Here, we use a comprehensive data set of *in situ* measurements performed over 2 years on the Argentière Glacier in the French Alps, complemented by state-of-the-art ice flow and hydrology modeling, to investigate changes in water storage at the ice-bedrock interface. We find strikingly large uplifts ranging between 0.20 and 0.90 m over the winter/spring seasons in the ablation zone. We show that this uplift is mostly related to enhanced bed separation as a result of increased basal water storage. We expect this study to be helpful to the glaciological community studying basal sliding and its modulation by sub-glacial hydrology with a view of improving predictions of the future behavior of mountain glaciers and outlet glaciers of ice sheets.

Key Points:

- We investigate horizontal, vertical velocities, basal sliding and subglacial runoff on the Argentière glaciers (French Alps)
- We find large uplifts ranging between 20 and 90 cm over the winter/spring seasons over a large part of ablation zone
- We show that the observed uplift is very likely related to enhanced bed separation as a result of increased storage of basal water

Supporting Information:

Supporting Information may be found in the online version of this article.

Correspondence to:

C. Vincent,
christian.vincent@univ-grenoble-alpes.fr

Citation:

Vincent, C., Gilbert, A., Walpersdorf, A., Gimbert, F., Gagliardini, O., Jourdain, B., et al. (2022). Evidence of seasonal uplift in the Argentière Glacier (Mont Blanc area, France). *Journal of Geophysical Research: Earth Surface*, *127*, e2021JF006454. https://doi.org/10.1029/2021JF006454

Received 1 OCT 2021
Accepted 29 JUN 2022

Author Contributions:

Conceptualization: Christian Vincent
Data curation: Christian Vincent, Andrea Walpersdorf, Olivier Gagliardini, Bruno Jourdain, Juan Pedro Roldan Blasco, Olivier Laarman, Luc Piard, Delphine Six, Luc Moreau, Diego Cusicanqui, Emmanuel Thibert
Formal analysis: Christian Vincent, Adrien Gilbert, Andrea Walpersdorf, Florent Gimbert, Olivier Gagliardini, Emmanuel Thibert
Investigation: Christian Vincent, Adrien Gilbert, Andrea Walpersdorf, Florent

1. Introduction

Glacier basal motion is responsible for a large part of ice flux in temperate alpine glaciers and outlet glaciers of ice sheets (Andrews et al., 2014; Bartholomaus et al., 2008; Fowler, 1987, 2015; Fountain & Walder, 1998; Lliboutry, 1968; Röthlisberger, 1972). However, the hydromechanical processes by which basal water controls sliding at the glacier bed are poorly known in large part because observations are very scarce (Clarke, 1996; Flowers, 2010; Fountain & Walder, 1998). Many studies have revealed a relationship between water input, from surface melting and rainfall, and increased ice-flow speed on mountain and outlet glaciers (e.g., Anderson et al., 2004; Bartholomew et al., 2011; Hoffman et al., 2016; Hooke et al., 1989; Howat et al., 2008; Iken & Bindschadler, 1986; Mair et al., 2002; Sugiyama & Gudmunsson, 2004). A common theory assumes that enhanced sliding results from increases in basal-water pressure due to the influx of water which overwhelms the

Gimbert, Olivier Gagliardini, Emmanuel Thibert
Methodology: Christian Vincent, Adrien Gilbert, Florent Gimbert
Project Administration: Christian Vincent
Software: Adrien Gilbert
Supervision: Christian Vincent
Validation: Christian Vincent
Writing – original draft: Christian Vincent, Florent Gimbert, Olivier Gagliardini
Writing – review & editing: Christian Vincent, Adrien Gilbert, Florent Gimbert, Olivier Gagliardini

capacity of the subglacial drainage system (Flowers, 2002; Harper et al., 2007; Lliboutry, 1968; Schoof, 2010). Theories make a distinction between two drainage systems, namely a slow, inefficient distributed drainage system consisting of cavities (Kamb, 1987; Walder, 1986) and a fast, efficient channelized system consisting of channels melted into the base of the ice (Nye, 1976; Röthlisberger, 1972). It is thought that dissipation of heat within the water flow in cavities can lead to the formation of channels. Depending on the nature of the bed substrate, channels can also be incised into the bedrock or sediments (Nye, 1973; Walder & Fowler, 1994).

The relationships between the sliding and the subglacial hydrology are complex given that the subglacial hydrologic network continuously adapts to the changing water supply through the formation or collapse of channels and cavities (e.g., Bartholomaus et al., 2008). Consequently, the hydraulic efficiency evolves dynamically, and continuous feedbacks occur between the ice dynamics and water flows. When water pressure increases to a threshold fraction of the overburden, cavities will form on the lee (down-glacier) side of bed obstacles, further reducing the basal drag exerted on the glacier base and increasing the sliding (Lliboutry, 1968). In this case, the drainage is inefficient. The main feedback of sliding is the opening of cavity space beyond bedrock bumps which lowers water pressure and in turn sliding (Bartholomaus et al., 2008; Flowers, 2015; Gimbert et al., 2021; Hoffman & Price, 2014; Jansson, 1995). The drainage becomes efficient when the channelized system forms and can drain large amounts of water. Efficiency declines again when channels and cavities collapse.

Despite these known general principles, many studies have shown that the spatio-temporal evolution of the subglacial hydrologic system remains poorly understood and they raise many issues. First, the spatial and temporal scales over which the basal drag influences the sliding are questionable. Several field-based studies have shown that the relationship between basal drag and glacier motion is apparent only over length scales of one to several ice thicknesses (Mair et al., 2001, 2002; Nienow et al., 2005). This corroborates the field observations of Iken and Bindschadler (1986) who state that the subglacial water pressure can affect the sliding velocity only if it acts on a large proportion of the glacier bed. Conversely, Sugiyama and Gudmunsson (2004) showed from field experiments at Lauteraargletscher, Switzerland, that the flow variations are mainly controlled by the local water pressure.

Second, other issues concern the relationships between sliding, water pressure and water storage. Some studies have suggested that sliding should be directly related to changes in water storage within the subglacial drainage system, rather than to water pressure (Harper et al., 2005, 2007; Kamb et al., 1994). These studies theorize that water storage in subglacial cavities leads to vertical motion of the glacier (uplift), which has been shown to be well correlated with increases in surface velocities and, by inference, basal motion on a number of glaciers (e.g., Anderson et al., 2004; Harper et al., 2007; Iken & Bindschadler, 1986; Kamb & Engelhardt, 1987; Sugiyama & Gudmunsson, 2004). However, Howat et al. (2008) noted that it is unclear whether bed separation varies with sliding speed in a more direct and consistent manner than water pressure varies with sliding speed. From their field observations at Breiðamerkurjökull (Iceland), they found a degree of hysteresis in the relationship between ice speed and basal separation that closely resembles the hysteresis often observed between ice speed and borehole-derived water pressures. Other studies have shown that basal sliding can open and connect subglacial cavities, even in the absence of extensive subglacial channelization (Bartholomaus et al., 2011; Hoffman & Price, 2014), increasing their ability to transport meltwater (Iken & Truffer, 1997) and reducing subglacial water pressures. In studies based on measurements in the Paakitsoq region of western Greenland, Andrews et al. (2014) found that decreasing trends in horizontal velocity during the end of the melting season are not related to the drainage efficiency of channelized systems, but may be caused by changes in connectivity in unchannelized regions. Hoffman et al. (2016) suggest a third weakly connected drainage component which would explain lowering ice speed during late summer despite little changes in water pressure during the latter part of the melt season.

Many questions about the current and future influence of increased surface melting on the dynamics of mountain glaciers and outlet glaciers of ice sheets remain unsolved. Answering these questions is crucial to predicting the behavior of glaciers and ice sheets in the future. Several studies in Greenland suggest that climate warming and enhanced surface melting could increase the sliding and enhance mass loss (Parizek & Alley, 2004; Zwally et al., 2002) while other studies suggest that an increase of melting could generate a more efficient subglacial drainage system draining large discharges in discrete channels, which could lead to a limited, or even reduced, effect on seasonally averaged sliding and the long-term dynamic response to a warming climate (Kamb, 1987; Pimentel & Flowers, 2010; Schoof, 2010; Sole et al., 2013; Sundal et al., 2011; Tedstone et al., 2015; Truffer et al., 2005; van de Wal et al., 2008).

Numerous studies highlight the paucity of field observations to investigate the relationships between the basal sliding and water storage or subglacial water pressure. A key variable needed to understand the relationships between the subglacial drainage system and sliding is the quantity of water that is stored at the interface between ice and bedrock. Previous studies tried to estimate variations in water storage from the difference between surface melt (or melt minus shallow subsurface refreezing) and discharge exiting the glacier (Bartholomaus et al., 2008) despite the large uncertainties. The water storage is also difficult to obtain accurately from uplift given that the uplift of ice is also potentially affected by the change in the vertical strain rates (Sugiyama & Gudmunsson, 2004), which are very difficult to estimate reliably.

Here, we investigate the relationships between horizontal and vertical velocities, basal sliding, subglacial runoff and ice-bed separation on the Argentière Glacier (French Alps). We determine the bed-separation and the quantity of water stored at the interface between ice and bedrock using the uplift approach. For this purpose, we use the comprehensive data set of in situ measurements performed in the ablation area over 2 years of continuous observations. We observe a strong surface uplift over the winter/spring seasons. We then correct this surface uplift by the influence of seasonal changes in strain rates and sliding velocity using ice-flow modeling, and conclude that the surface uplift observed in winter/spring is mostly caused by an underlying bed separation increase of similar amplitude.

2. Data and Methods

2.1. Study Area

The Argentière Glacier is located in the Mont-Blanc mountain range in the French Alps (45°55′ N and 6°57′E). Its surface area was approximately 10.9 km^2 in 2018 (Figure 1). The glacier extends from an altitude of approximately 3,400 m a.s.l. at the upper bergschrund down to 1,600 m a.s.l. at the snout and is about 10 km long. The debris cover can be 0.05–0.10 m thick in some locations. The field observations of the Argentière Glacier (i.e., mass-balance, thickness variations, ice-flow velocities, and length fluctuations over 50 years) come from the French glacier-monitoring program called GLACIOCLIM (Les GLACIers, un Observatoire du CLIMat; https://glacioclim.osug.fr/). For the present study, additional detailed observations were carried out in the framework of the SAUSSURE program (Sliding of glAciers and sUbglacial water preSSURE [https://saussure.osug.fr]). Note that Horace Bénédict de Saussure (1740–1799), naturalist, performed many scientific studies in the Alps and proposed prize money in 1786 to those capable of reaching the summit of Mont Blanc for the first time.

Our study focuses on a small area of Argentière Glacier (~0.2 km^2) located between 2,320 and 2,400 m a.s.l. in the ablation zone (Figure 1). In this area, the ice is generally free of debris. The glacier is ~600 m wide, the horizontal ice-flow velocity is ~55 m a^{-1} (Vincent et al., 2009, 2021) and the maximum ice thickness is 250 m (Gimbert et al., 2021; Rabatel et al., 2018). Experiments conducted in boreholes (Hantz & Lliboutry, 1983) indicate that the bed is composed of hard rock with no thick and deforming sediment layer.

2.2. Data

Surface ice-flow velocities and point-mass balances were monitored between 2018 and 2020 using a network of ablation stakes (Figure 1) composed of 17 stakes (1, 2, 4–12, and 14–19) spatially distributed over the selected area and 14 stakes (A–N) aligned along a longitudinal profile in two different sectors, designated as upper (A–G) and lower (H–N) sectors in this paper. The ablation stakes were 10 m long and made of five sections, each two m long, tied together with metal chains. The stakes were replaced each year and were always set up at the same locations, using a hand-held GPS device (accuracy of ±10 m), to ensure comparison. Geodetic measurements were repeatedly performed to obtain the 3D coordinates of the ablation stakes over the monitoring period. For this purpose, we used a Leica 1200 Differential Global Positioning System (GNSS) unit, running with dual frequencies. Occupation times were typically 1 min with 1-s sampling and the number of visible satellites (GPS and GLONASS) was always greater than seven. The distance between the fixed receiver and the mobile receiver was less than 1 km. The DGPS positions have an intrinsic accuracy of ±0.01 m. However, depending on the size of the holes drilled to insert the stakes, the stake positions are accurate to ±0.05 m. The DGPS measurements were performed simultaneously with the stakes readings (visible length of the stakes) in order to obtain the exact position of the bottom tip of the stake from the buried length of the stake, given that the total length of each stake is known. In this manner, it was possible to monitor ice velocity along the three coordinate directions.

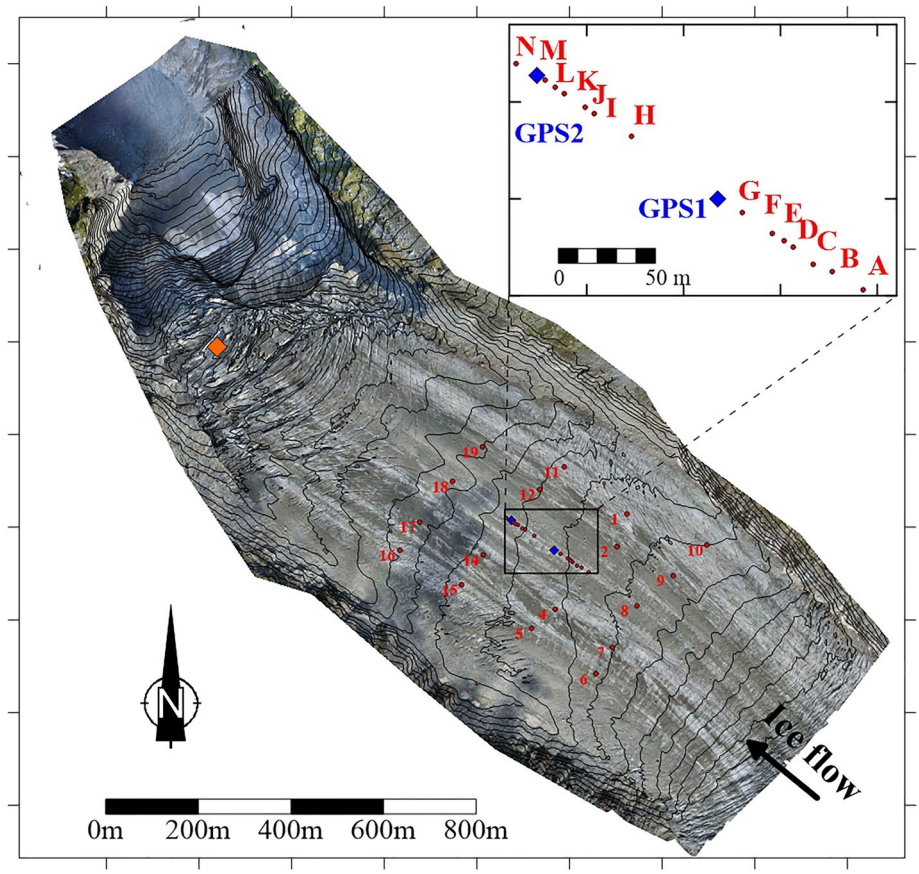

Figure 1. Network of stakes used to study the changes in ice-flow velocities and the uplift over the years 2018–2020 on the Argentière Glacier. The red dots show the ablation stakes distributed over the entire studied area including the ablation stakes set up on a longitudinal profile. The orange diamond shows the position of the cavitometer used for the basal-sliding measurements and water discharge measurements. The blue dots correspond to the stakes set up in April 2019, on which DGPS antennas were set up to measure the daily horizontal and vertical velocities.

The vertical velocity is the vertical component of the surface velocity obtained from stake measurements. It is obtained from the altitude differences of the bottom tip of the stake between two consecutive measurements. Depending on the tilt of the ablation stakes, the size of the drilling hole and the mechanical play of the jointed stakes, we assumed that the annual horizontal and vertical velocities were accurate to within ± 0.10 m a^{-1}, when the measurements are performed on the entire year.

Errors in ablation measurements are essentially due to the mechanical play of the jointed stakes. The uncertainties of the annual mass-balance measurements performed in this ablation zone were estimated to be 0.14 m w.e. a^{-1} (Thibert et al., 2008).

The measurements were performed with time intervals varying between 10 days and 3 months (Table 1). Due to the COVID 19 lockdown in France in 2020, field campaigns were canceled between March and May 2020. During the winter/spring season (December to May), snow accumulation reached thicknesses exceeding 3 m. Consequently, pits had to be dug to find the stakes under the snow and to measure the positions of each stake on the basis of GNSS measurements. For this reason, only five stakes were measured in both March and May.

In addition to these repeatedly measured stake positions, continuous GNSS measurements were performed on two sites, GPS1 and GPS2, located on the longitudinal profile (Figure 1). The GNSS antennas were installed on 4 or 5 m aluminum masts anchored between 2 and 3 m deep in the ice and thus emerging above the surface. The masts were reinstalled several times during the summer season due to the high melting rate. The measurements were carried out using Leica GR25 receivers from the French national receiver parc (https://gpsmob.resif.fr). The registered GNSS data consist of multi-frequency GPS, GLONASS, and GALILEO signals at 1 s intervals. These

Table 1
Time Schedule of Measurements

	Year 2018				Year 2019										Year 2020							
Date	5/9	3/10	23/10	11/12	22 /3	6 /5	19/6	4/7	25/7	11/8	13/09	4/10	23/10	3/12	31/1	7/5	23/6	23/7	12/8	9/9	18/9	29/10
Surface mass balance																						
DGPS																						
UAV Photog.																						

Note. The dark-blue cells correspond to the surface mass-balance and DGPS measurements performed on the whole network of ablation stakes. The light blue cells correspond to the measurements performed on the longitudinal profile only. The green cells indicate the Unmanned Aerial Vehicle (UAV) photogrammetric measurements

data were analyzed in a regional network of 13 fixed reference stations from the RENAG network (http://renag.resif.fr) at distances between 3 and 180 km. Average daily positions have a formal uncertainty of 1 and 5 mm on the horizontal and vertical components, respectively, yielding annual velocity uncertainties ranging between 0.5 and 2.5 m.a^{-1}. Theses measurements were started in April 2019 and were maintained until the summer of 2021.

Geodetic surveys of the glacier surface were conducted on 5 September 2018, 13 September 2019, and 18 September 2020 using the senseFly eBee + Unmanned Aerial Vehicle to obtain digital elevation models (DEMs). A total of 720 photos in 2018, 673 in 2019, 646 in 2020 were collected with the onboard senseFly S.O.D.A. camera (20 Mpx RGB sensor with a 28 mm lens from an average altitude of 140 m above the glacier surface). Prior to the survey flights, we collected DGPS measurements of ground control points (GCPs) that consisted of rectangular red pieces of cloth (1.00 × 0.60 m) with painted white circles (0.40 m diameter) on the glacier (10 in 2018, 20 in 2019, and 12 in 2020) and ten 0.40 m diameter white circles painted on rocks on the ridges of the glacier. The original resolutions of the orthomosaic and DEMs were 0.10 and 1.00 m respectively. The images from the survey were processed using the Structure for Motion (SfM) algorithm that is implemented in the software package Agisoft Metashape Professional version 1.6 (Smith et al., 2015). The SfM stereo technique was then used to generate a dense point cloud of the glacier surface. This dense point cloud was used to construct the DEMs using the GCP data collected during the field campaigns. A detailed description of the processing steps can be found in Kraaijenbrink et al. (2016) or Brun et al. (2016).

Finally, thanks to the tunnels drilled through the rock beneath the glacier in the 1970s by the hydroelectric power company Emosson S.A., the sliding movement and the subglacial runoff have been measured nearly continuously since 1989 (Gimbert et al., 2021; Vincent & Moreau, 2016). The sliding velocity is measured at 2,173 m a.s.l. in a cavity that opens behind a bedrock bump using a "cavitometer" designed by Vivian (1975). The cavitometer consists of a bicycle wheel with a circumference of 1.55 m attached to a 1.30 m articulated arm that is attached to the rock. The accuracy of the daily sliding velocity measurements has been assessed to be better than ±0.01 m d^{-1} (Vincent & Moreau, 2016). The subglacial runoff is monitored in another tunnel at 2,060 m a.s.l. during the summer season using an Endress Hauser sensor which measures the water level in a calibrated channel. The subglacial runoff is measured with an accuracy of ±0.1 m^3 s^{-1}. The measurement frequency is 15 min. The cavitometer and runoff measurements are described in detail in Vincent and Moreau (2016).

2.3. Principle of Calculation of the Ice-Bed Separation Compared to Schemes From Previous Studies

In the case of a hard bed, "bed separation" is assumed to represent the water storage close to the bed (Iken et al., 1983). It can be determined by the uplift of the surface. However, two different types of uplift sources should be distinguished, namely the uplift caused by vertical deformation of the ice column and the uplift caused by the increase in volume of subglacial water cavities (Anderson et al., 2004; Harper et al., 2007; Hooke et al., 1989; Mair et al., 2002; Sugiyama & Gudmunsson, 2004). "Bed separation" is therefore calculated by removing both

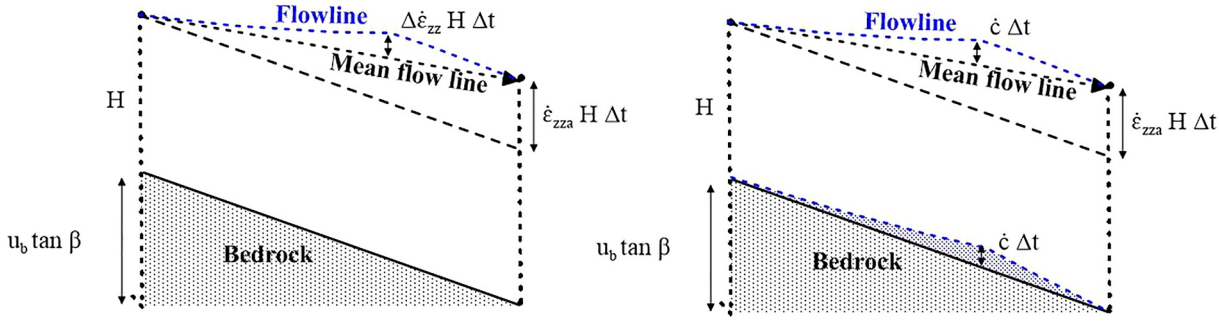

Figure 2. Direction of the flowline in a vertical plane between October of the first year and October of the second year. The seasonal uplift is the result of (a) the vertical displacement $\Delta u_b \tan \beta\, \Delta t$ related to the sliding change Δu_b, (b) the strain-rate change $\Delta\, \dot{\varepsilon}_{zz}\, H\, \Delta t$ (illustrated on the left panel) and (c) the bed separation $\dot{c}\, \Delta t$ (illustrated on the right panel). Note that the flow is compressive in this example.

the downward vertical component of bed-parallel displacement and the vertical motion due to ice strain from the measured vertical position time series.

The vertical velocity w_s obtained from surface measurements (DGPS or classical topography) is expressed as (Hooke et al., 1989):

$$w_s = u_b \tan \beta + \dot{\varepsilon}_{zz}\, H + \dot{c} \tag{1}$$

where β is bed slope and u_b is the horizontal component of the sliding velocity. Thus, $u_b \tan \beta$ is the downward vertical component of mean bed-parallel motion. $\dot{\varepsilon}_{zz}$ is the vertical-strain rate averaged over the glacier thickness and $\dot{c}$ is the vertical component of basal cavity opening rate or "bed separation."

We integrate Equation 1 to calculate displacement due to bed separation over a time step Δt:

$$\Delta z_s = u_b \tan \beta \Delta t + \dot{\varepsilon}_{zz}\, H\, \Delta t + \dot{c}\, \Delta t \tag{2}$$

Given that vertical-strain rate $\dot{\varepsilon}_{zz}$ and sliding velocity are not constant over time, Equation 2 can be written as following:

$$\Delta z_s = u_{ba} \tan \beta \Delta t + \Delta u_b \tan \beta \Delta t + \dot{\varepsilon}_{zza}\, H\, \Delta t + \Delta\, \dot{\varepsilon}_{zz}\, H\, \Delta t + \dot{c}\, \Delta t \tag{3}$$

where u_{ba} is the sliding averaged over the whole year, Δu_b is the deviation of the sliding from the annual average, $\dot{\varepsilon}_{zza}$ is the vertical-strain rate averaged over the glacier thickness and over the whole year, and $\Delta\, \dot{\varepsilon}_{zz}$ is the deviation of the vertical-strain rate from the annual average. In our study, the seasonal uplift is the result of (a) the vertical displacement $\Delta u_b \tan \beta\, \Delta t$ related to the sliding change, (b) the strain-rate change $\Delta\, \dot{\varepsilon}_{zz}\, H\, \Delta t$, and (c) the bed separation $\dot{c}\, \Delta t$.

The last two terms of the uplift, $\Delta\, \dot{\varepsilon}_{zz}\, H\, \Delta t$ and $\dot{c}\, \Delta t$ are shown in Figure 2, for the sake of clarity.

Several studies have attempted to determine bed separation in mountain glaciers or outlet glaciers of the Greenland Ice Sheet (see Table S1 in Supporting Information S1). One of the most famous early studies on uplift of mountain glaciers is that of Iken et al. (1983). They documented an upward movement of up to 0.6 m in the Unteraargletscher (Switzerland). They interpreted these observations as the result of cavity growth at the glacier bed in response to pressurized water, pointing out the influence of water pressure on the glacier sliding speed. However, they did not consider the influence of variations in the vertical-strain rate (Flowers, 2010). To isolate the bed separation $\dot{c}$ (Equation 1), most studies suggest removing (a) vertical strain and (b) bed-parallel motion from the vertical motion w_s obtained from surface geodetic measurements (e.g., Anderson et al., 2004; Harper et al., 2007; Hoffman et al., 2011; Howat et al., 2008; Mair et al., 2002; Sugiyama & Gudmunsson, 2004). To that end, an estimation of the vertical-strain rate is needed. In many studies, the vertical-strain rate $\dot{\varepsilon}_{zz}$ is assumed to be uniform with depth and is calculated using the surface horizontal-strain rate (Anderson et al., 2004; Andrews et al., 2018; Hoffman et al., 2011; Howat et al., 2008; Iken & Bindschadler, 1986; Mair et al., 2001). However, it is known that the vertical-strain rate $\dot{\varepsilon}_{zz}$ can vary significantly with depth (Balise & Raymond, 1985; Blatter, 1995; Lliboutry, 1995; Sugiyama & Gudmunsson, 2004; Ryser et al., 2014), although very few studies

have measured directly the internal vertical-strain rate from borehole length measurements (Iken et al., 1996; Sugiyama & Gudmunsson, 2004) or other instruments (Young et al., 2019). The bed-parallel motion is obtained from measurements of bed slope using Ground Penetrating Radar or seismic techniques or borehole drillings, and assessment of sliding (Anderson et al., 2004; Harper et al., 2007; Howat et al., 2008). Given that the slope of the bed is subject to great uncertainty, other studies suggest calculating the bed-parallel motion as a residual from winter conditions assuming that the components of bed-parallel motion and vertical strain are constant and the basal-uplift rate is zero during the winter season (Andrews et al., 2018; Hoffman et al., 2011; Sugiyama & Gudmunsson, 2004). In these latter studies, the authors assume that the bed slope is uniform over the distance traveled during the observation window. Note that this assumption has not been checked, and part of the observed uplifts could be due to a bump in the bedrock. Given that the uplift is generally less than 0.2 m, the results of these studies are questionable. In addition, most of these studies neglected the fact that part of the observed changes in vertical displacement are due to changes in glacier sliding velocity occurring on a sloping bed, which corresponds to the term $\Delta u_b \tan \beta\, \Delta t$ in Equation 2.

Here, we propose to determine the sum of two terms ($u_{ba} \tan \beta\, \Delta t + \dot{\varepsilon}_{zza} H\, \Delta t$) of Equation 3 on the basis of annual measurements. This sum can be calculated directly from the vertical displacement Δz_s on the annual scale, assuming that the annual vertical motion of ice is not affected by changes in the basal sliding, strain rate and bed separation on the annual scale. Subtracting this sum from Equation 3, one can obtain the uplift ($\Delta u_b \tan \beta\, \Delta t + \Delta \dot{\varepsilon}_{zz} H\, \Delta t + \dot{c}\, \Delta t$) very accurately from the DGPS measurements.

The method is similar to that of Sugiyama and Gudmunsson (2004), Hoffman et al. (2011), and Andrews et al. (2018). However, in order to avoid assuming that the bed slope is uniform over the distance traveled during the observation window and in order to make measurements independent of bed slope, we performed measurements on several stakes set up over very short distances apart on a longitudinal profile as shown in Figure 1. We observed the same uplift simultaneously at several stakes over a distance of a few tens of meters, meaning that the uplift was not due to the presence of bedrock bumps (see Section 3.1). In light of these results, we are confident that our method can correctly determine the total uplift.

However, our method outlined so far does not allow us to distinguish the effect of bed separation from those of changes in the vertical strain rate or changes in the vertical displacement $\Delta u_b \tan \theta\, \Delta t$ related to the sliding seasonal change. Determining the changes in the vertical-strain rate over the period of measurements is a complicated task given that (a) vertical-strain rates can change over the considered period given that the glacier moves non-uniformly, and (b) the vertical-strain rate varies with depth and the assessment of $\Delta\, \dot{\varepsilon}_{zz}$ from the surface horizontal-strain rates is likely a poor approximation. Similarly, the changes in the vertical displacement $\Delta u_b \tan \beta\, \Delta t$ related to the changes in seasonal sliding seasonal change cannot be obtained directly from the surface observations. Thus, for this determination, we combine numerical ice-flow modeling with the in situ observations.

2.4. Numerical Modeling Procedure

We use numerical modeling to quantify the extent with which the observed uplift may be due to the change in sliding speed on a sloping bed (term $\Delta u_b \tan \beta\, \Delta t$ in Equation 2) and the change in vertical deformation of ice (term $\Delta\, \dot{\varepsilon}_{zz} H\, \Delta t$ in Equation 2). Our numerical model thus does not include a representation of uplift due to cavitation, which we aim to infer a posteriori from the discrepancies between the predicted and the observed uplift. We use the finite element software Elmer/Ice (Gagliardini et al., 2013) to solve for the coupling between ice flow and basal hydrology. For the ice flow, the Stokes equations are solved without approximation which makes possible the quantification of all components of the strain-rate tensor everywhere in the glacier. To initialize the model, we use a bed topography DEM with high resolution (10 m) in the area of interest, which has been obtained through repeated radar surveys conducted in 2018 (Gimbert et al., 2021), and glacier surface DEMs acquired by stereo photography in 1998 and 2003. Ice viscosity is assumed to be spatially uniform and set to the usual value for temperate ice assuming a non-linear Glen's flow law with an exponent $n = 3$ (Cuffey & Paterson, 2010). Basal friction is estimated according to the formulation proposed in Thøgersen et al. (2019) where friction is modeled in a transient way following a "rate-and-state" approach with:

$$\tau_b = \left(\frac{u_b}{A_s}\right)^{\frac{1}{m}} (1 - \theta(t)), \tag{4}$$

where τ_b is basal shear stress (MPa), u_b the sliding velocity (m a^{-1}), A_s the friction coefficient, m the sliding exponent, and θ a dimensionless state parameter that describes the degree of cavitation. The evolution of θ is given by:

$$\frac{d\theta}{dt} = \frac{u_b}{d_c}(\theta - \theta^*), \tag{5}$$

where d_c is a characteristic length scale corresponding to the typical length of cavities (set to 2 m) and θ^* the value of θ at steady state, which is linked to effective pressure N and sliding speed following Gagliardini et al. (2007) as:

$$\theta^* = 1 - \left(\frac{1}{1+\alpha\chi^q}\right)^{1/m} \text{ with } \chi = \frac{u_b}{(CN)^m A_s} \text{ and } \alpha = \frac{(q-1)^{q-1}}{q^q} \tag{6}$$

where q and C are parameters that are function of bed roughness characteristics. We use field constrained parameter values for C, q, and m provided by Gimbert et al. (2021) based on the analysis of long-term basal sliding measurements at the wheel location. We estimate the friction coefficient field A_s for the entire glacier from surface velocity inversion performed using the September 2003 surface velocity field inferred from SPOT5 satellite image correlation (Berthier et al., 2005). Alternatively, we also performed an inversion of ice viscosity for uniform A_s with the same data set in order to perform an additional simulation and evaluate the impact of ice viscosity on our results. We used the coupling of basal friction with subglacial hydrological to compute effective pressure using the GlaDS model (Werder et al., 2013) as described in Gagliardini and Werder (2018). Both ice flow and GlaDS are solved using a finite element method within Elmer/Ice which allows an integrated coupling where ice flow and subglacial hydrology are iteratively solved for a given effective pressure and sliding velocity, respectively. The evolutions of the free surface and melt water input at the glacier base are computed from a surface mass balance model proposed by Oerlemans (2001) which includes the effect of potential short wave radiation variability. The mass balance model is forced by daily temperature and precipitation taken from the Safran reanalysis (Vernay et al., 2021), and is calibrated from the GLACIOCLIM monitoring network data (https://glacioclim.osug.fr/) over the period 1975–2020 in order to reproduce both spatial and temporal variability of the measured surface mass balance. We assume that surface melting is directly supplied to the glacier bed. The timestep is set to 48 min for the subglacial hydrology and 4 days for the ice dynamics. Sub-daily melting rate used to force the subglacial hydrology model is obtained from hourly temperature time series also available from the Safran reanalysis. The hydro-mechanical model has been calibrated using sliding speed observed in situ over a 20-year period (2000–2020) (Gilbert et al., 2021). To ensure glacier geometry is physically consistent, we started the simulation in 2000 letting the surface relax according to the surface mass balance and the modeled ice dynamics before reaching the period of interest of this study (2018–2020). The three-dimensional velocities and strain rates are extracted from the numerical model every month to evaluate their spatio-temporal changes.

In addition to this reference simulation where A_s is inverted and the ice viscosity is uniform, we perform three simulations to evaluate the sensitivity of our results to changes in friction and in ice viscosity. We thus run the same simulation with (a) uniform A_s and inverted ice viscosity and (b) a simplified description of the seasonal frictional changes. This simplified approach is done by using only two uniform values of A_s in which the switch between the two values is determined by the occurrence or not of surface melting. We apply this approach for two different values of uniform ice viscosity: (a) with the standard temperate ice viscosity and (b) by doubling the flow rate factor in the Glen's law.

3. Results

3.1. Evidence of Uplift From Vertical Movements

Horizontal and vertical ice-flow velocities were observed regularly over two hydrologic years between September 2018 and October 2020 (Table 1) using the network of stakes. We report the detailed movement of the stakes B, I, GPS1, GPS2 during the years 2018/2019 and the stakes B′ and GPS1 during the year 2019/2020 on a longitudinal section (Figure 3). The horizontal velocities range from 42 to 58 m a^{-1} in the central region during the winter and summer seasons respectively. Between September 2018 and September 2020, the thickness decreased by about 4.7 m in this region. The annual vertical velocities were studied thoroughly in this region in a previous study (Vincent et al., 2021) in which it was shown that they can be positive or negative. As shown in Figure 3 (bottom panel), the vertical velocities are positive in the upper part of the profile and negative in the lower part.

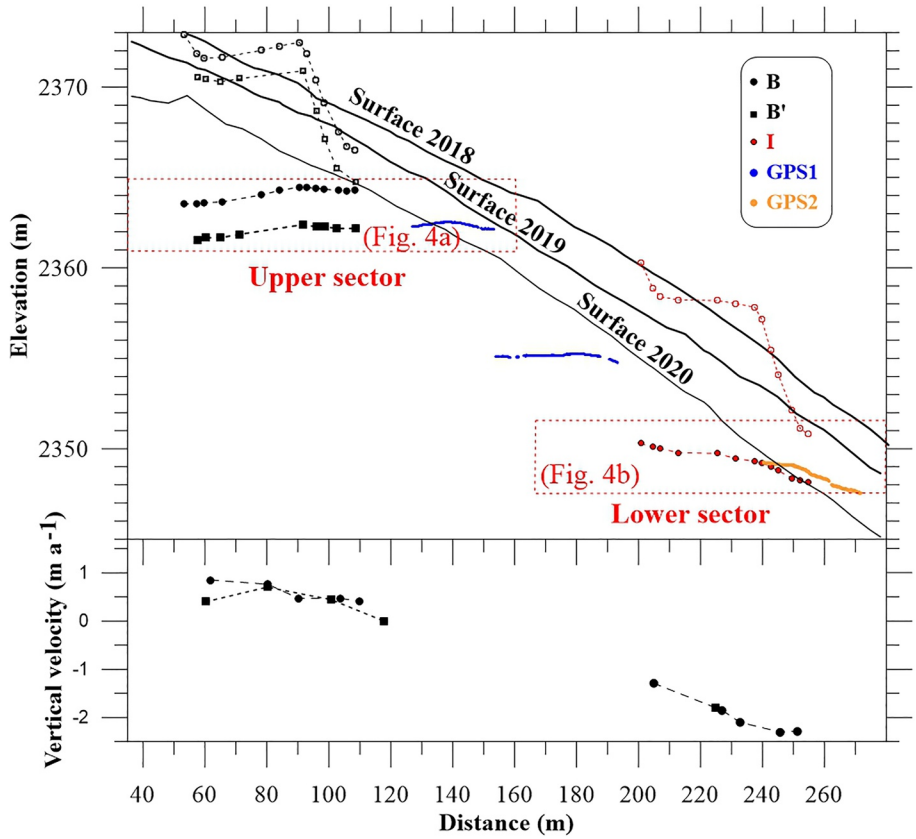

Figure 3. Longitudinal cross section showing the movement of stakes B (observed in 2018/2019), B′ (observed in 2019/2020), and I (observed in 2018/2019). The surfaces 2018, 2019, and 2020 correspond to the elevation of the ice in September 2018, September 2019, and September 2020. The stakes were measured 13 times during the year 2018/2019 and 9 times during the year 2019/2020. For each stake and each date, we reported the positions of the bottom of the stake (filled dots) and those of the surface of the ice (unfilled dots). The blue and orange dots show the continuous DGPS measurements GPS1 and GPS2 performed since April 2019. For the sake of clarity, the other stakes of the longitudinal profile (Figure 1) are shown in Figures 4a and 4b for which the boundaries are shown here (squared red dashed lines). The annual vertical velocities calculated from the stakes located on the longitudinal profile (Figure 1) are plotted in the bottom panel.

The change in surface elevation depends on the surface mass balance and the emergence velocity (Cuffey & Paterson, 2010). In the ablation zone, the emergence velocities are positive, which corresponds to an upward flow of ice relative to the glacier surface at a fixed x, y coordinates. During the winter season when melting is reduced, the elevation of the ice surface increases (Figure 3). Other stakes shown in Figure 1 have not been reported in Figure 3 for the sake of clarity, but are depicted in the magnified Figure 4. The vertical trajectories of these stakes are not linear and reveal waves which correspond to non-uniform and/or time-dependent vertical velocities (Figure 3). The maximum values of uplift are reached simultaneously for all stakes on 9 June 2019 and 23 June 2020 as highlighted in Figure 4a by downward arrows. The minimum values are reached for all stakes at the beginning of December 2018 and December 2019. These observations indicate that local bumps in bedrock topography are not a potential cause of vertical uplift and argue in favor of a temporal effect related to a large-scale seasonal uplift.

We note that the upward movement starts at the beginning of December in both hydrologic years and ends in June. It is also the case in the lower part of the longitudinal profile (Figure 4b) although this pattern is less visible as a result of annual vertical velocities being negative there.

3.2. Analysis of Seasonal Changes of Horizontal and Vertical Velocities, Sliding, Runoff, and Uplift

The surface horizontal and vertical ice-flow velocities are reported in Figures 5 and 6 separately for the two sectors (Figure 4), for the sake of clarity and because the annual mean vertical velocities are significantly different

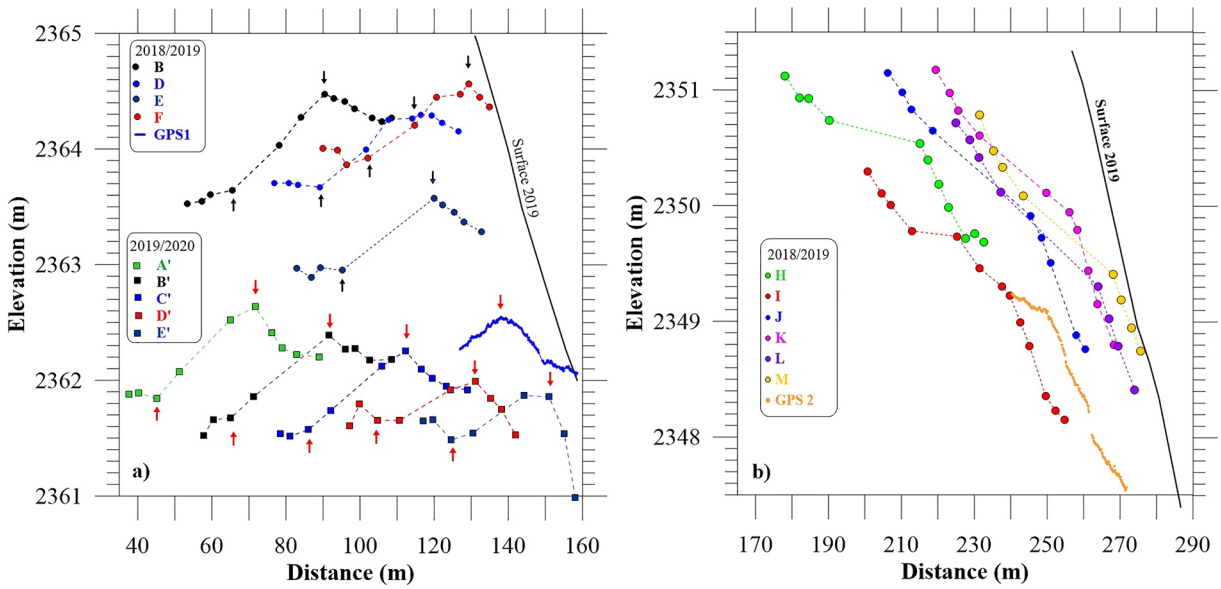

Figure 4. Longitudinal cross sections showing the displacement of the bottom tip of stakes in (a) the upper sector for the 2 years and (b) the lower sector for the year 2018/2019. The two sectors are depicted in Figures 1 and 3. Note that the measurements were performed 15 to 21 times between 5 September 2018 and 29 October 2020 for the ablation stakes and between 1 April 2019 and 17 November 2019 continuously for the stakes GPS1 and GPS2. The upward black and red arrows show the observations performed on 11 December 2018 and 3 December 2019, respectively. The downward black and red arrows show the observations performed on 9 June 2019 and 23 June 2020, respectively.

in these two sectors. Note that the measurements in the second sector were performed during the year 2018–2019 only. The January to July uplifts of the stakes located on the longitudinal profile range between 0.40 and 0.60 m (Figures 5d and 6c).

A detailed analysis of Figure 5 reveals the following features.

- First, the surface horizontal velocities show an acceleration, which starts very early in December 2018 and 2019, with peaks between June and July for the two hydrologic years, respectively (Figure 5a). This period shows that, although the sliding velocity decreases at the wheel location between December and end of April, the surface horizontal velocity is observed to increase higher up (about 800 m from the wheel). Note however that the thickness of ice increases over this period due to positive emergence velocities, snow falls and no melting (Figure 5f). Thus, this thickness increase could explain part of the increase in the surface horizontal velocity through enhanced driving stress causing greater ice deformation. The influence of this enhanced ice deformation will be analyzed later from ice flow modeling (Section 3.4). Note also that the sliding and surface velocities not being measured at the same place could also explain the observed differences. We also investigate this potentiality later on (Section 4.1).
- Second, after the beginning of May 2019, a strong acceleration corresponds to a large increase in the sliding speed (Figures 5a and 5b). For the following hydrologic year 2019/2020, the increase in sliding speed started earlier in the season, in April 2020, was less abrupt and led to a smoother acceleration in the surface horizontal velocity. During these periods of horizontal acceleration, that is, between December and June, the vertical velocity was higher than the annual average and led to an uplift of the surface (Figures 5c and 5d). However, the vertical velocity started to decrease after the beginning of May, which stabilized the uplift during the months of May and June.
- Third, during June 2019 (May and June 2020), the surface horizontal velocity and the sliding velocity were close to their maximum. After the beginning of August 2019 (beginning of July 2020), the surface horizontal velocity and the sliding velocity declined until the end of November. Note also that the thickness is strongly affected by the melting rate during this period (Figure 5f). The vertical velocity behaves slightly differently. After the beginning of July (2019 and 2020), the vertical velocities drop and reach values less than the annual average which leads to a lowering of the surface until the beginning of November. Note that the vertical

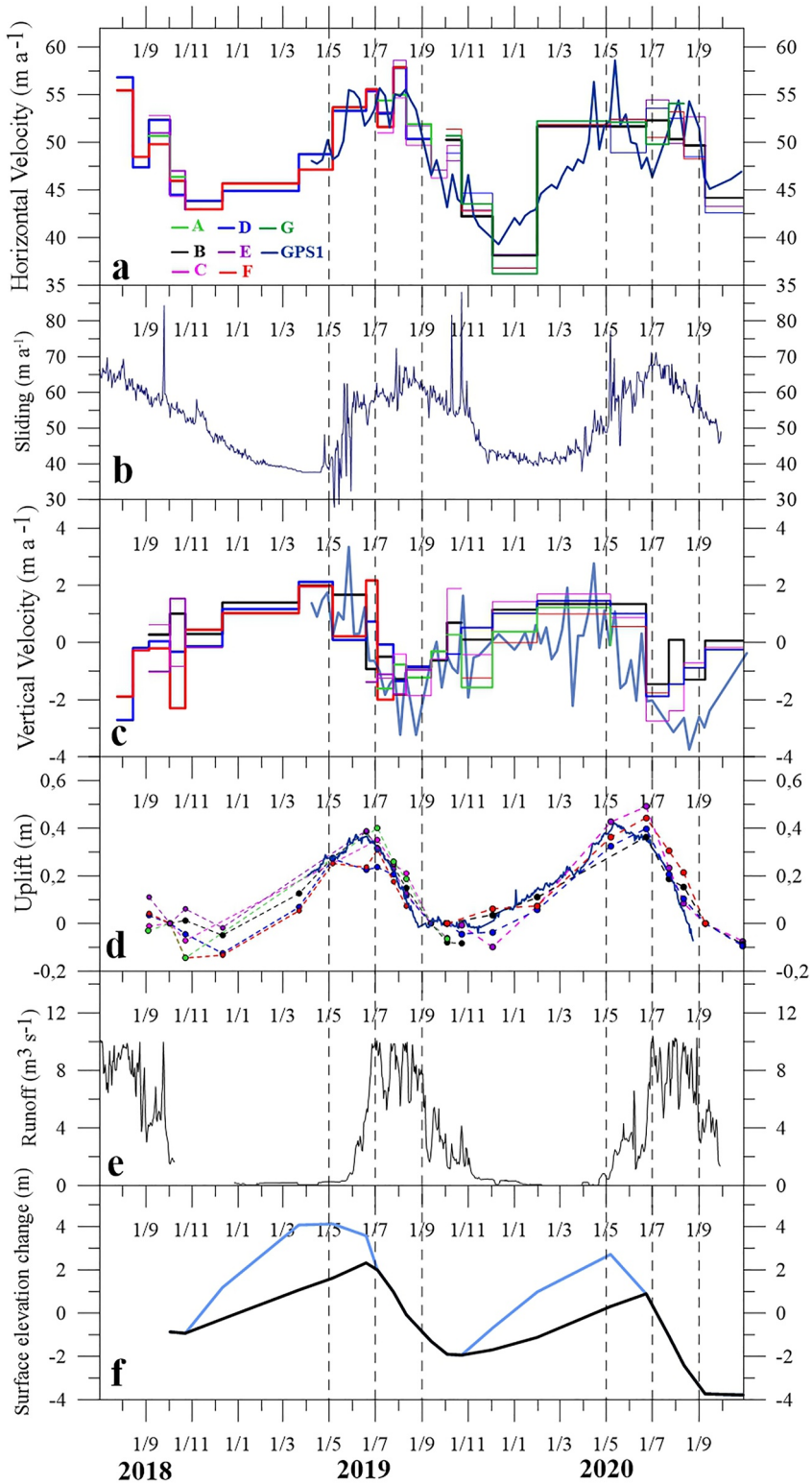

Figure 5. (a) Horizontal velocities observed on the upper longitudinal section shown in Figure 3a, (b) sliding velocities obtained from the subglacial measurements performed using the wheel, (c) vertical velocities observed on the upper longitudinal section, (d) uplift calculated from the vertical displacements, (e) runoff monitored in the subglacial observatory at 2,060 m a.s.l., and (f) surface elevations changes of ice (black) and snow (blue) calculated using the surface data from September 2018 and September 2019. The blue line shows the height of snow above the surface of ice (black line) which is expressed in meters of snow. The velocities obtained from continuous measurements at GPS1 (blue in panels (a and c)) were calculated on a weekly time scale.

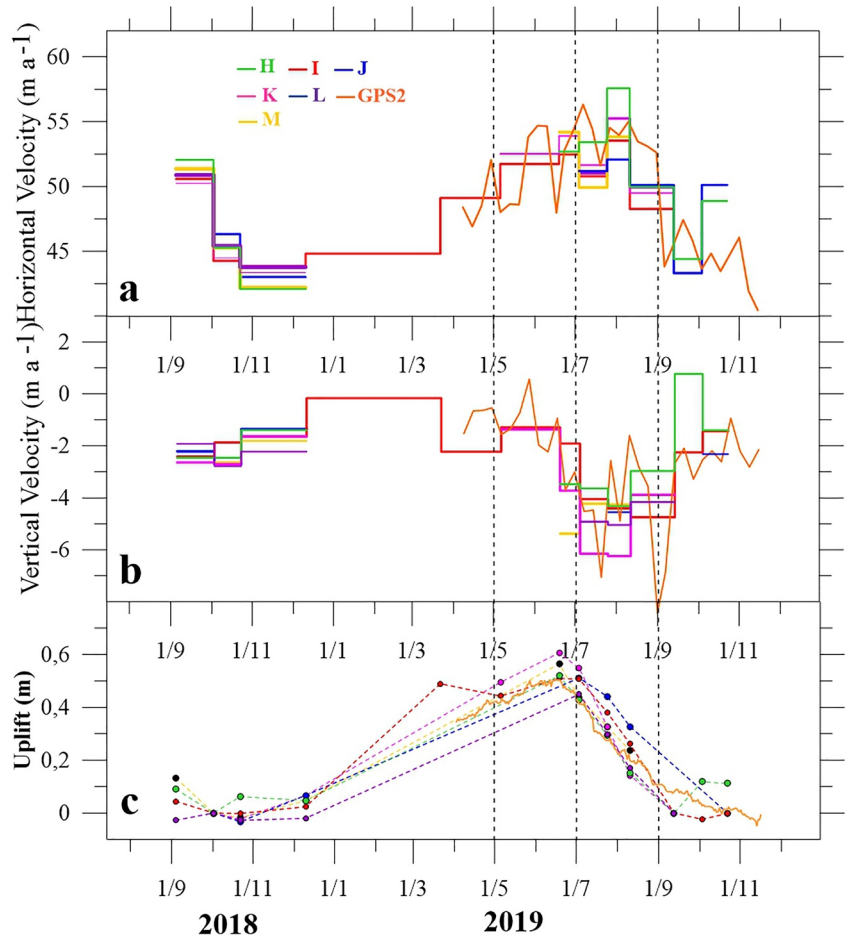

Figure 6. (a) Horizontal and (b) vertical velocities observed during the year 2018/2019 on the lower longitudinal section shown in Figure 3b, (c) uplift calculated on the basis of the annual and seasonal vertical velocities. The velocities obtained from continuous measurements at GPS2 were calculated (i) for periods similar to those of the stakes, and (ii) on a weekly time scale.

velocities increase again between the beginning of August and December, but are not able to produce an uplift given that they remain below the annual average.

- Fourth, the subglacial runoff, reported in Figure 5d, shows that, on the seasonal time scale, there is a clear relationship between sliding and runoff, that is, similar oscillations of sliding velocity and runoff. A detailed examination reveals that the sliding velocity increased greatly at the beginning of the melt season in May (2019 and 2020), before the large increase in runoff at the beginning of June (2019 and 2020). However, there is a small but increasing level of runoff recorded from the beginning of May when the sliding velocity starts to increase. In addition, the sliding velocity continued to decrease after the runoff fell back to low values less than 5 m^3/s at the beginning of September.
- Fifth, the behaviors of vertical velocities and uplifts were very similar and homogeneous over the two hydrologic years with some variations in the timing. Similar patterns were observed over the lower part of the longitudinal profile (Figure 6).

3.3. Spatial Patterns of Uplift

As shown in the previous section, the magnitude of the uplift was very similar (0.4–0.6 m) for each stake located on the longitudinal profile (Figures 5d and 6c). In this section, we analyze the surface uplift across our entire stake network (Figures 1, 7a, and 7b). The measurements performed on the entire network are not as complete as those made along the longitudinal profile due to lack of measurements during the winter/spring seasons between

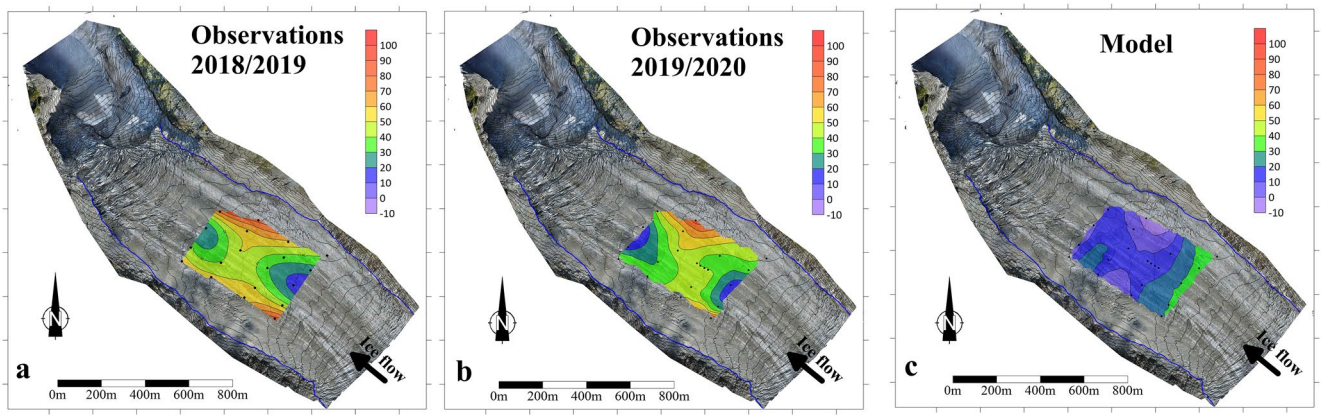

Figure 7. Spatial pattern of uplift (in cm), using the entire network of stakes (a) observed between 3 October 2018 and 4 July 2019, and (b) observed between 13 September 2019 and 23 June 2020, and (c) calculated from numerical modeling. These modeled uplifts result from sliding and strain rate changes only.

3 October 2018 and 4 July 2019 and between 3 December 2019 and 23 June 2020. Fortunately, this lack of completeness does not affect the results for the total uplift given that the maximum was reached close to the beginning of July for these two years (Figure 5). Our results reveal uplifts ranging between 0.20 and 0.90 m over the entire observed zone (Figures 7a and 7b).

The uplift is at a minimum in the central part of the glacier where the glacier is the thickest. The uplift is greater closer to the edges of the glacier. A striking feature is the similarity of the spatial pattern over 2019 and 2020, which shows the repeatability of our observations.

3.4. Modeled Seasonal Ice Flow Variations

As explained in Section 2.3, the uplifts observed during the two winter/spring periods (Figures 7a and 7b respectively) can have three different, but possibly superimposing, sources. Uplift can be due to (a) the change in sliding speed on a sloping bed (term $\Delta u_b \tan \beta \, \Delta t$ in Equation 2), (b) the change in vertical deformation of ice (term $\Delta \dot{\varepsilon}_{zz} \, H \, \Delta t$ in Equation 2), and/or (iii) the growth of subglacial water cavities (term $\dot{c} \, \Delta t$ in Equation 2). Here, we use the three-dimensional coupled model introduced in Section 2.4 to evaluate the contribution of the first two terms and thus conclude whether cavity growth $\dot{c}$ needs to be invoked in order to explain our uplift observations.

The numerical modeling results are reported in Figure 8. We compared the observed and calculated surface horizontal and vertical velocities as well as the surface elevation change over the period 2018–2020 (Figures 8a–8c, respectively) at the GPS1 stake, located close to the center of our network (Figure 1). We found a relatively good agreement with the observed surface horizontal velocities (Figure 8a), in particular during the melt period, when water is supplied to the bed (May to October). However, the comparison of the observed and calculated vertical velocities reveals large discrepancies (Figure 8b). Although the seasonal variation of the average surface vertical velocity is well represented, predicted amplitudes remain much smaller than observed ones.

We computed the spatial pattern of the vertical velocity anomaly (Figure 8e) from the difference between the vertical velocity over October 2018–June 2019 period and the annual average (Figure 8d). We then calculated the resulting uplift by integrating the vertical velocity anomaly over time during this same period in order to compare it with the observed one (Figure 7c). We recall that this modeled uplift results from the combination of change in sliding velocity and strain rate only. The analysis of the vertical strain rate and its winter/spring anomaly (Figures 8f and 8g) highlights that strain changes are very small and are not responsible for the vertical velocity anomaly in the model, which is rather explained by changes in sliding speed at the glacier bed. This is also well illustrated in the longitudinal cross sections presented in Figure S1 and S2 in Supporting Information S1 where the vertical velocity anomalies at the bed are similar to the ones at the surface in this region. The model allowed us to predict an uplift of at most 0.2 m (Figure 7c) which is significantly smaller than the observed ones (Figures 7a and 7b). We conclude that the pattern of the modeled vertical velocity anomalies (Figure 8e) and the associated calculated uplift (Figure 7c) mainly reflect changes in sliding velocity on a sloping bedrock and do not match the observed uplift (Figures 7a and 7b).

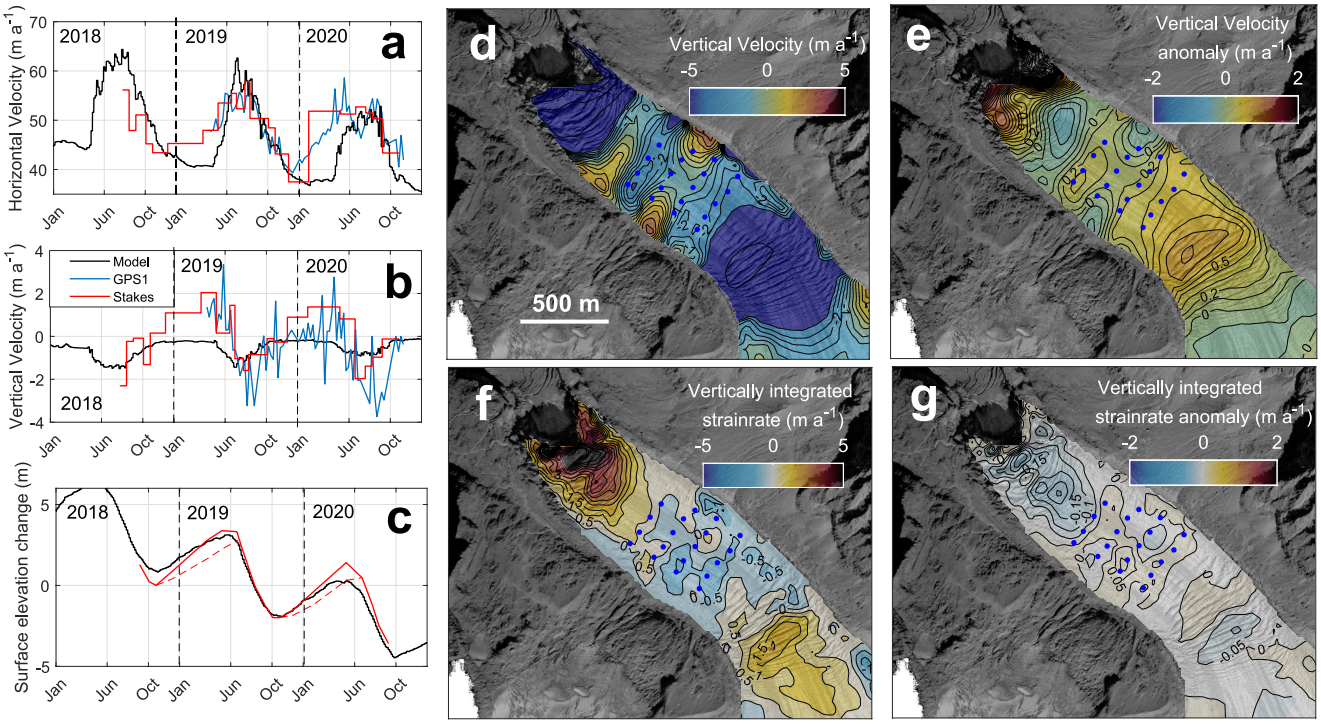

Figure 8. (a) Comparison between modeled (black lines) and observed (red and blue lines) surface horizontal velocities, (b) modeled and observed vertical velocities and (c) elevation change, at the GPS1 location. Spatial pattern of (d) mean annual vertical velocities, (e) vertical velocity anomalies over the October 2018–June 2019 period compared to the annual average, (f) mean annual vertically integrated strain rates, and (g) vertically integrated strain rate anomalies over the October 2018–June 2019 period. Positive values in panel (f) are vertical compression. Note that, in panel (c), the snow surface (red line) is shown with the snow height converted in meters of ice.

In addition, the discrepancies between observed and modeled surface horizontal velocities from December to May reveals that bed shear stress increase due to increased glacier thickness as well represented in the model (Figure 8c), is not responsible for the observed horizontal velocity increase. An increase in ice thickness of 3 m ice-equivalent, as observed in Figure 8c, leads to, at most, an increase of 3 m a^{-1} in the horizontal velocity in the studied area. Thus, an additional process likely related to the subglacial hydrology needs to be invoked.

Finally, we test if the predicted uplift is sensitive to spatial changes in friction and/or ice viscosity to evaluate the robustness of our finding. For this purpose, we perform sensitivity tests by (a) using an inverted viscosity field and uniform As, (b) using a simple frictional change when surface melting occurs instead of using the hydrological model and, (c) by doubling the flow rate factor in the Glen's law of the test (see also Section 2.4). These complementary numerical experiments (see Supporting Information S1) show calculated uplifts that are of similar magnitude to those predicted previously (Figure S3 and S4 in Supporting Information S1), which gives confidence that the effect of sliding velocity and strain rate changes cannot explain the observed uplift, consistent with cavity growth being needed to explain the observations.

In order to estimate the contribution of the basal uplift to that observed at the surface, we used the model outputs to derive a regression between modeled surface vertical and horizontal velocities at the location of the upper stake network (A–G). This regression ($R^2 = 0.96$) allows us to estimate, as a function of the surface horizontal velocity, the amount of surface vertical velocity due to changes in strain rate and sliding velocity. By applying this relationship to the observed horizontal velocities, we calculate the vertical velocities due to strain rate and sliding changes which we remove from the measured surface vertical velocities in order to retrieve the basal vertical velocities. We finally calculate the basal uplift from time integrating the basal vertical velocities, which we refer to as the reconstructed basal uplift (Figure 9a).

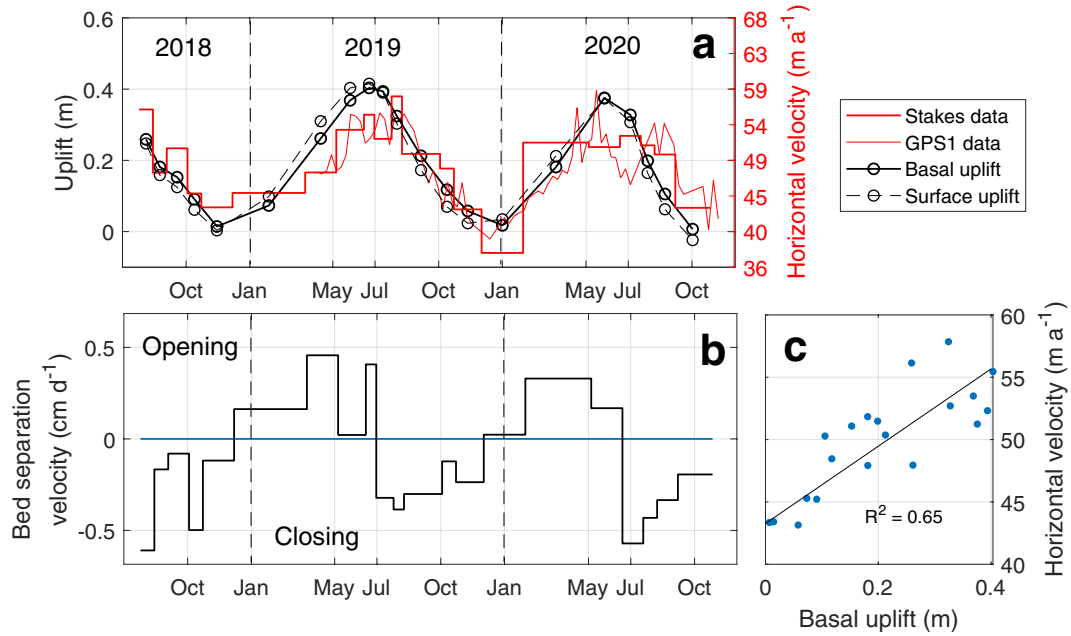

Figure 9. (a) Comparison between observed horizontal velocities (in red), measured uplift at the glacier surface (dashed black line) and reconstructed uplift at the glacier base (bold black line). The uplifts observed from the stakes (Figure 5d) have been averaged over all stakes. The reconstructed basal uplift is obtained from the difference between the measured surface uplift and the uplift due to strain rate and sliding changes. (b) Reconstructed basal separation velocity. (c) Correlation between reconstructed basal uplift and observed surface horizontal velocities.

4. Discussions

4.1. Methods and Uncertainties Relating to the Determination of Bed Separation

Several difficulties and uncertainties must be addressed when quantifying bed separation from observations of glacier surface uplift.

The uplift Δz_s (Equation 2) is usually measured from inferring the vertical displacements of stakes (Anderson et al., 2004; Andrews et al., 2018; Bartholomaus et al., 2011; Bartholomew et al., 2012; Harper et al., 2007; Hoffman et al., 2011; Howat et al., 2008; MacGregor et al., 2005). However, because stakes also move according to the ice flow on top of a sloping bed, most studies assume that the bed slope β does not change over the distance traveled by the stakes. In other words, it relies on assuming that the first term on the right-hand side of Equation 2, "$u_b \tan \beta \, \Delta t$", is constant. Other studies obtain the value of the bed slope from GPR measurements (e.g., Howat et al., 2008) or calculate the uplift from the upward change on the detrended height profile by comparison with annual observations (Bartholomew et al., 2012). As done in our study, we advise setting up several stakes at very short distances apart along the same flow line to make sure that the observed uplift is not related to the presence of a bedrock bump over the distance traveled by the stakes.

Quantifying bed separation on the basis of surface uplift observations also requires removing the effect of temporal changes in bed sliding velocity (term $\Delta u_b \tan \beta \, \Delta t$ in Equation 3) and vertical strain rate (term $\Delta \, \dot{\varepsilon}_{zz} \, H \, \Delta t$ in Equation 3). This task is particularly challenging. Several studies neglect the temporal variations in the vertical strain rate (e.g., Iken et al., 1983). Most studies assess vertical strain rates from surface horizontal strain rates obtained from measurements on a network of stakes (Anderson et al., 2004; Andrews et al., 2018; Armstrong & Anderson, 2020; Harper et al., 2007; Hoffman et al., 2011; Howat et al., 2008; MacGregor et al., 2005). These studies assume that the vertical strain rate is depth-invariant although most of these studies recognize that this is likely not the case, as shown in several other studies (Balise & Raymond, 1985; Blatter, 1995; Lliboutry, 1995; Ryser et al., 2014; Sugiyama & Gudmunsson, 2004) and confirmed by our modeling.

Here, we addressed these issues by using a three-dimensional ice-flow model that is calibrated based on a wide range of field observational constraints using surface velocity fields, high resolution three-dimensional bed

DEMs, basal sliding velocity observations and surface mass balance observations. The use of this model enabled us to calculate the contributions of thickness-integrated vertical strain rates and basal sliding changes to the observed surface uplift under various model assumptions.

We find that the contributions of vertical strain rates and basal sliding changes are small, such that the observed surface uplift (see Figure 5d and the dashed black line in Figure 9a) is very similar to the the reconstructed basal uplift (see continuous line in Figure 9a). The uncertainty on the reconstructed basal uplift is due to the uncertainty on the measured surface vertical velocity, which is estimated to be lower than 0.1 m a^{-1} (5 cm of uncertainty on the uplift amplitude), the reliability of the derived relationship between surface vertical and horizontal velocities and the quality of the regression. The error introduced by the regression would be uniform in time and thus does not affect the velocity anomaly used to quantify the uplift. The uncertainty associated with the modeled vertical velocity can be significant when looking at the absolute value (see Figure S2b in Supporting Information S1) but remains low regarding the relative changes that are used to quantify uplift. The standard deviation of the simulated uplifts across the different tests (Figures S2 and S3 in Supporting Information S1) is of about 5 cm and can be taken as an estimation of the error associated with model predictions. The total uncertainty on the reconstructed basal total uplift is thus expected to be lower than 10 cm, with 5 cm coming from surface observations and 5 cm from the model, giving a basal uplift value over the period January–July estimated to be of 40 $\pm$ 10 cm at the upper stakes center line.

4.2. Evidence for Cavity Growth as a Likely Mechanism to Explain the Observed Uplift

We suggest that cavity growth is likely the main process responsible for the increase in basal uplift inferred from January to June. We support this assertion with three independent lines of evidence. First, the basal uplift time series is well correlated with the horizontal velocity time series (Figures 9a and 9c), consistent with the classical theoretical conceptualization that cavity growth simultaneously lifts the basal ice interface and increases surface horizontal velocities through enhanced sliding (Gagliardini et al., 2007; Lliboutry, 1968; Schoof, 2005). Note however that the decrease in sliding observed from the wheel located 800 m downstream, between October and the beginning of May (Figure 5b), is opposite of what is observed in the stakes/GPS area investigated here. This could reflect different basal hydrology conditions over these two regions of the glacier. Second, the bed separation velocity time series calculated from time differentiating the inferred basal uplift (Figure 9b) exhibits (a) amplitudes on the order of 0.5 cm/day which are typical of cavity opening and closing rates for a sliding velocity of about 10 m a^{-1} as estimated at the measurement site (Werder et al., 2013), and (b) a temporality that closely matches that previously observed in basal water pressure measurements (see Figure 5c of Nanni et al., 2020), with a positive trend being particularly marked from October to January. Third, subglacial-runoff observations suggest that water supply to the glacier bed during the uplift time period is largely sufficient for filling up cavities of the size required by our observations. Integrating subglacial water discharge from January to June yields a volume of water of about 15×10^6 m^3 in the ablation zone, which corresponds to about 2.7 m when evenly distributed over the entire 5.5 $\pm$ 1 km^2 glacier ablation zone. Since this value is much larger than the 0.5 m uplift observed presently, water supply to the glacier bed is likely largely sufficient for filling up cavities of the size required to explain our uplift observations (Figure 10).

4.3. Influence of Enhanced Surface Melting on the Dynamics

The questions related to the impact of enhanced surface melting and meltwater input on the future of mountain glaciers and outlet glaciers of ice sheets remain unclear. Several studies related to the outlet glaciers of the Greenland Ice Sheet suggest that enhanced surface melting could increase sliding and generate a positive feedback to mass loss as faster flow causes the ice sheet to lower into warmer elevations (Parizek & Alley, 2004; Zwally et al., 2002). Other studies suggest that the subglacial drainage system could adapt to variable meltwater inputs (Bartholomaus et al., 2008; Iken & Bindschadler, 1986; Mair et al., 2002) that is, a more efficient subglacial drainage system could lead to large discharges in discrete channels which could generate a limited, or even decelerating, effect on seasonally averaged sliding and the long-term dynamic response to a warming climate (Bartholomew et al., 2011; Hoffman et al., 2011; Kamb, 1987; Pimentel & Flowers, 2010; Schoof, 2010; Sundal et al., 2011; Truffer et al., 2005; van de Wal et al., 2008).

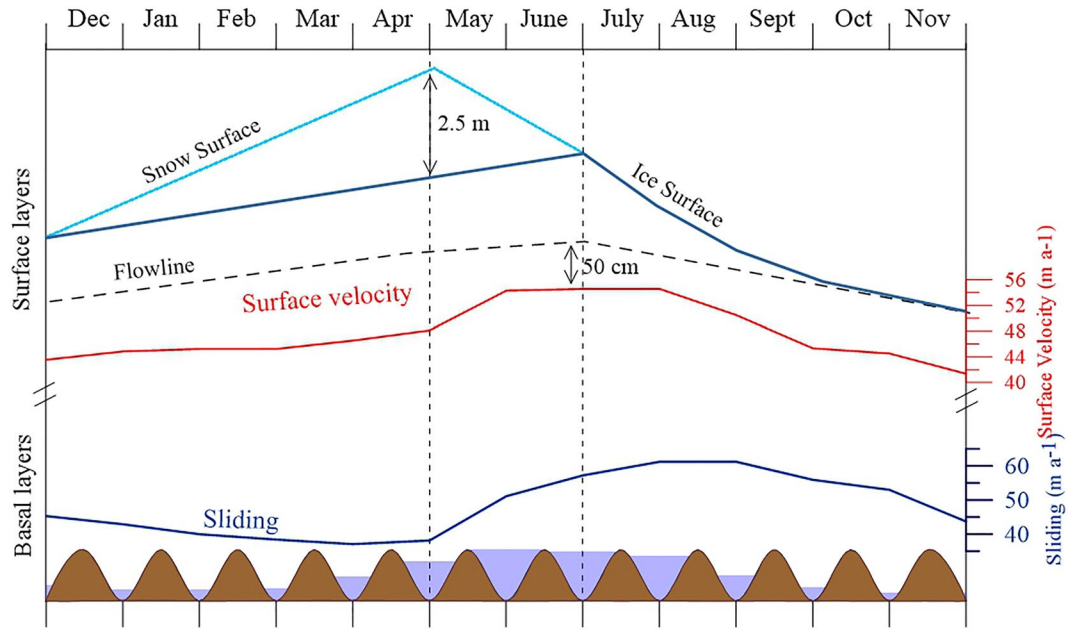

Figure 10. Sketch of a possible scenario of basal and surface conditions during the year. Here, the uplift is 0.50 m and related to the bed separation. Note that the reported sliding is measured at the wheel location about 800 m from the stakes network.

In our study, we found that the horizontal velocity increased greatly before the increase in runoff at the beginning of the melt season in May which seems indicative of an inefficient subglacial drainage system. Between the beginning of July and the end of August, we observed large sliding velocities which could mean that the subglacial channels cannot absorb the large water input coming from the surface melting. However, the sliding and surface horizontal velocities decrease progressively from September to November although the runoff falls back suddenly at the beginning of September after the end of the main melting season, which suggests a progressive closing of subglacial channels and reducing the efficiency of the drainage. Thus, our observations suggest a limitation of summer ice velocity as soon as water easily drains to the ice-bed interface and a very slow and gradual decline of ice velocity by September. This later decrease could reflect a conflict between a positive feedback on sliding related to the decrease of the drainage efficiency and a negative feedback on sliding related to the increase in basal drag.

One can conclude that the increase in water input coming from the melting will in the future lead to a peak velocity earlier in the summer, but will not necessarily change the dynamics of the sliding.

5. Conclusions

This study allowed us to investigate the horizontal and vertical velocities, the basal sliding, the subglacial runoff and the bed separation, stemming from a comprehensive continuous data set of in situ measurements acquired at Argentière Glacier over 2 years.

The surface horizontal velocities show an acceleration which starts very early in December. They increase abruptly at the beginning of May and peak between June and July for the two investigated hydraulic years, 2018–2019 and 2019–2020, respectively. During these periods of horizontal acceleration, that is, between December and June, the vertical velocity is higher than the annual average. The vertical velocities start to decrease from the beginning of May and drop suddenly below the annual average after the beginning of July. After the beginning of August (2019/July in 2020), the surface horizontal velocity declined until the end of November.

Our method and observations enabled us to identify with great confidence striking uplifts ranging between 0.20 and 0.90 m over the winter/spring seasons between January and June and over a large part of the ablation zone. Such uplifts, which are obviously not dependent on the surface accumulation or ablation rates, have rarely been

observed on glaciers. These seasonal uplifts could have three different sources, namely a change in sliding speed on a sloping bed, vertical straining of ice or an increase in the volume of subglacial cavities. Quantifying bed separation on the basis of surface uplift observations requires removing the effect of temporal changes in bed sliding velocity and in vertical strain rate, which is particularly challenging. We addressed these issues by using a three-dimensional ice-flow model that is calibrated based on a wide range of field observational constraints using surface velocity fields, high resolution three-dimensional bed DEMs, basal sliding velocity observations and surface mass balance observations. From observations and ice-flow modeling, we find that the changes in sliding speed on a sloping bed and the strain-rate changes cannot explain the observed uplift rates. Consequently, the uplift is very likely related to enhanced bed separation as a result of increased storage of basal water. We found that more than 80% of the observed uplift is related to enhanced bed separation through cavitation. In addition, we found a good correlation between the surface horizontal velocities and the bed separation which supports our observations and modeling and is consistent with the classical theory.

In conclusion, the uplift observed at Argentière Glacier is very likely related to enhanced bed separation as a result of increased basal-water storage. In the future, inclinometric observations in boreholes would be needed to fully estimate the changes in strain rates and quantify the sliding speed at the observation site.

Conflict of Interest

The authors declare no conflicts of interest relevant to this study.

Data Availability Statement

The digital elevation model data can be accessed from https://zenodo.org/record/3556552#.YVRp3LgzZPY (Jourdain, 2019). The horizontal, vertical ice-flow velocities and calculated uplift can be accessed from https://zenodo.org/record/5536953#.YVRvGLgzZPY (Vincent, 2021).

Acknowledgments
This study was funded by the *Agence Nationale de la Recherche* in the framework of the SAUSSURE program (Sliding of glAciers and sUbglacial water pressure [https://saussure.osug.fr] (ANR 18 CE1 0015 01)) and the *Observatoire des Sciences de l'Univers de Grenoble* (OSUG) and the *Institut des Sciences de l'Univers* (INSU-CNRS) in the framework of the French GLACIOCLIM (*Les GLACIers, un Observatoire du CLIMat*) program. The authors thank the French national GNSS receivers network (https://gpsmob.resif.fr). The authors thank all those who conducted the field measurements. The authors are grateful to Cary Bartsch for reviewing the English. The authors thank Martin Luethi and two anonymous reviewers whose thorough comments improved the quality of the manuscript. The authors are indebted to the associate Editor at *JGR* for reading the manuscript carefully and helping to improve it.

References

Anderson, R. S., Anderson, S. P., MacGregor, K. R., Waddington, E. D., O'Neel, S., Riihimaki, C. A., & Loso, M. G. (2004). Strong feedbacks between hydrology and sliding of a small Alpine glacier. *Journal of Geophysical Research*, *109*(F3), F03005. https://doi.org/10.1029/2004JF000120

Andrews, L., Catania, G. A., Hoffman, M. J., Gulley, J. D., Luethi, M. P., Ryser, C., et al. (2014). Direct observations of evolving subglacial drainage beneath the Greenland Ice Sheet. *Nature*, *514*(7520), 80–83. https://doi.org/10.1038/nature13796

Andrews, L. C., Hoffman, M. J., Neumann, T. A., Catania, G. A., Lüthi, M. P., Hawley, R. L., et al. (2018). Seasonal evolution of the subglacial hydrologic system modified by supraglacial lake drainage in western Greenland. *Journal of Geophysical Earth Surface*, *123*(6), 1479–1496. https://doi.org/10.1029/2017JF004585

Armstrong, W. H., & Anderson, R. S. (2020). Ice-marginal lake hydrology and the seasonal dynamical evolution of Kennicott Glacier, Alaska. *Journal of Glaciology*, *66*(259), 1–15. https://doi.org/10.1017/jog.2020.4

Balise, M., & Raymond, C. (1985). Transfer of basal sliding variations to the surface of a linearly viscous glacier. *Journal of Glaciology*, *31*(109), 308–318. https://doi.org/10.3189/S002214300000664X

Bartholomaus, T. C., Anderson, R. S., & Anderson, S. P. (2008). Response of glacier basal motion to transient water storage. *Nature Geoscience*, *1*(1), 33–37. https://doi.org/10.1038/ngeo.2007.52

Bartholomaus, T. C., Anderson, R. S., & Anderson, S. P. (2011). Growth and collapse of the distributed subglacial hydrologic system of Kennicott Glacier, Alaska, USA, and its effects on basal motion. *Journal of Glaciology*, *57*(206), 985–1002. https://doi.org/10.3189/002214311798843269

Bartholomew, I., Nienow, P., Sole, A., Mair, D., Cowton, T., & King, M. A. (2012). Short-term variability in Greenland Ice Sheet motion forced by time-varying meltwater drainage: Implications for the relationship between subglacial drainage system behavior and ice velocity. *Journal of Geophysical Research*, *117*(F3), F03002. https://doi.org/10.1029/2011JF002220

Bartholomew, I., Nienow, P., Sole, A., Mair, D., Cowton, T., Palmer, S., & Wadham, J. (2011). Supraglacial forcing of subglacial drainage in the ablation zone of the Greenland Ice Sheet. *Geophysical Research Letters*, *38*(8), L08502. https://doi.org/10.1029/2011GL047063

Berthier, E., Vadon, H., Baratoux, D., Arnaud, Y., Vincent, C., Feigl, K. L., et al. (2005). Surface motion of mountain glaciers derived from satellite optical imagery. *Remote Sensing of Environment*, *95*(1), 14–28. https://doi.org/10.1016/j.rse.2004.11.005

Blatter, H. (1995). Velocity and stress fields in grounded glaciers: A simple algorithm for including deviatoric stress gradients. *Journal of Glaciology*, *41*(138), 333–344. https://doi.org/10.3189/S002214300001621X

Brun, F., Buri, P., Miles, E. S., Wagnon, P., Steiner, J., Berthier, E., et al. (2016). Quantifying volume loss from ice cliffs on debris-covered glaciers using high resolution terrestrial and aerial photogrammetry. *Journal of Glaciology*, *62*(234), 684–695. https://doi.org/10.1017/jog2016.542016

Clarke, G. K. C. (1996). Lumped-element analysis of subglacial hydraulic circuits. *Journal of Geophysical Research*, *101*(B8), 17547–17559. https://doi.org/10.1029/96Jb01508

Cuffey, K. M., & Paterson, W. S. B. (2010). *The physics of glaciers* (4th ed., p. 693). Elsevier.

Flowers, G. E. (2002). A multicomponent coupled model of glacier hydrology 1. Theory and synthetic examples. *Journal of Geophysical Research*, *107*(B11), 2287. https://doi.org/10.1029/2001JB001122

Flowers, G. E. (2010). Glacier hydromechanics: Early insights and the lasting legacy of three works by Iken and colleagues. *Journal of Glaciology*, *56*(200), 1069–1078. https://doi.org/10.3189/002214311796406103

Flowers, G. E. (2015). Modelling water flow under glaciers and ice sheets. *Proceedings of the Royal Society A*, *471*(2176), 20140907. https://doi.org/10.1098/rspa.2014.0907
Fountain, A. G., & Walder, J. S. (1998). Water flow through temperate glaciers. *Reviews of Geophysics*, *36*(3), 299–328. https://doi.org/10.1029/97RG03579
Fowler, A. C. (1987). A theory of surge. *Journal of Geophysical Research*, *92*(B9), 9111–9120. https://doi.org/10.1029/jB092iB09p09111
Gagliardini, O., Cohen, D., Råback, P., & Zwinger, T. (2007). Finite-element modeling of subglacial cavities and related friction law. *Journal of Geophysical Research*, *112*(F2), F02027. https://doi.org/10.1029/2006JF000576
Gagliardini, O., & Werder, M. (2018). Influence of increasing surface melt over decadal timescales on land-terminating Greenland-type outlet glaciers. *Journal of Glaciology*, *64*(247), 700–710. https://doi.org/10.1017/jog.2018.59
Gagliardini, O., Zwinger, T., Gillet-Chaulet, F., Durand, G., Favier, L., de Fleurian, B., et al. (2013). Capabilities and performance of Elmer/Ice, a new-generation ice sheet model. *Geoscientific Model Development*, *6*(4), 1299–1318. https://doi.org/10.5194/gmd-6-1299-2013
Gilbert, A., Gimbert, F., Thøgersen, K., Schuler, T. V., & Kääb, A. (2021). Consistent framework for coupling basal friction with subglacial hydrology on hard-bed glaciers. *Geophysical Research Letters*, e2021GL097507. https://doi.org/10.1029/2021GL097507
Gimbert, F., Nanni, U., Roux, P., Helmstetter, A., Garambois, S., Lecointre, A., et al. (2021). A multi-physics experiment with a temporary dense seismic array on the Argentière Glacier, French Alps: The RESOLVE Project. *Seismological Research Letters*, *92*(2A), 1185–1201. https://doi.org/10.1785/0220200280
Hantz, D., & Lliboutry, L. (1983). Waterways, ice permeability at depth and water pressures at glacier d'Argentière, French Alps. *Journal of Glaciology*, *29*(102), 227–238. https://doi.org/10.3189/S0022143000008285
Harper, J. T., Humphrey, N. F., Pfeffer, W. T., Fudge, T., & O'Neel, S. (2005). Evolution of subglacial water pressure along a glacier's length. *Annals of Glaciology*, *40*, 31–36. https://doi.org/10.3189/172756405781813573
Harper, J. T., Humphrey, N. F., Pfeffer, W. T., & Lazar, B. (2007). Two modes of accelerated glacier sliding related to water. *Geophysical Research Letters*, *34*(12), L12503. https://doi.org/10.1029/2007GL030233
Hoffman, M., & Price, S. (2014). Feedbacks between coupled subglacial hydrology and glacier dynamics. *Journal of Geophysical Research: Earth Surface*, *119*(3), 414–436. https://doi.org/10.1002/2013JF002943
Hoffman, M. J., Andrews, L. C., Price, S. F., Catania, G. A., Neumann, T. A., Lüthi, M. P., et al. (2016). Greenland subglacial drainage evolution regulated by weakly connected regions of the bed. *Nature Communications*, *7*(1), 13903. https://doi.org/10.1038/ncomms13903
Hoffman, M. J., Catania, G. A., Neumann, T. A., Andrews, L. C., & Rumrill, J. A. (2011). Links between acceleration, melting, and supraglacial lake drainage of the Western Greenland Ice Sheet. *Journal of Geophysical Research*, *116*(F4), F04035. https://doi.org/10.1029/2010JF001934
Hooke, R., Calla, P., Holmlund, P., Nilsson, M., & Stroeven, A. (1989). A 3 year record of seasonal variations in surface velocity, StorglaciÄren, Sweden. *Journal of Glaciology*, *35*(120), 235–247. https://doi.org/10.3189/S0022143000004561
Howat, I. M., Tulaczyk, S., Waddington, E., & Björnsson, H. (2008). Dynamic controls on glacier basal motion inferred from surface ice motion. *Journal of Geophysical Research*, *113*(F3), F03015. https://doi.org/10.1029/2007JF000925
Iken, A., & Bindschadler, R. A. (1986). Combined measurements of subglacial water pressure and surface velocity of the Findelengletscher, Switzerland: Conclusions about drainage system and sliding mechanism. *Journal of Glaciology*, *32*(110), 101–119. https://doi.org/10.3189/S0022143000006936
Iken, A., Fabri, K., & Funk, M. (1996). Water storage and subglacial drainage conditions inferred from borehole measurements on Gornergletscher, Valais, Switzerland. *Journal of Glaciology*, *42*(141), 233–248. https://doi.org/10.3189/S0022143000004093
Iken, A., Röthlisberger, H., Flotron, A., & Haeberli, W. (1983). The uplift of Unteraargletscher at the beginning of the melt season—A consequence of water storage at the bed? *Journal of Glaciology*, *29*(101), 28–47. https://doi.org/10.3189/S0022143000005128
Iken, A., & Truffer, M. (1997). The relationship between subglacial water pressure and velocity of Findelengletscher, Switzerland, during its advance and retreat. *Journal of Glaciology*, *43*(144), 328–338. https://doi.org/10.3189/S0022143000003282
Jansson, P. (1995). Water pressure and basal sliding on Storglaciaren, northern Sweden. *Journal of Glaciology*, *41*(138), 232–240. https://doi.org/10.3189/S0022143000016130
Jourdain, B. (2019). DEM and orthophoto Argentiere Glacier – 13/09/2019 (V1.2) [Dataset]. Zenodo. https://doi.org/10.5281/zenodo.3556552
Kamb, B. (1987). Glacier surge mechanism based on linked cavity configuration of the basal water conduit system. *Journal of Geophysical Research*, *92*(B9), 9083–9099. https://doi.org/10.1029/JB092iB09p09083
Kamb, B., & Engelhardt, H. (1987). Waves of accelerated motion in a glacier approaching surge: The mini-surges of Variegated Glacier, Alaska, U.S.A. *Journal of Glaciology*, *33*(113), 27–46. https://doi.org/10.3189/s0022143000005311
Kamb, B., Engelhardt, H., Fahnestock, M. A., Humphrey, N., Meier, M., & Stone, D. (1994). Mechanical and hydrologic basis for the rapid motion of a large tidewater glacier: 2. Interpretation. *Journal of Geophysical Research*, *99*(B8), 15231–15244. https://doi.org/10.1029/94JB00467
Kraaijenbrink, P. D. A., Immerzeel, W. W., Pellicciotti, F., de Jong, S. M., & Shea, J. M. (2016). Object-based analysis of unmanned aerial vehicle imagery to map and characterise surface features on a debris-covered glacier. *Remote Sensing of Environment*, *186*, 581–595. https://doi.org/10.1016/j.rse.2016.09.013
Lliboutry, L. (1968). General theory of subglacial cavitation and sliding of temperate glaciers. *Journal of Glaciology*, *7*(49), 21–58. https://doi.org/10.3189/S0022143000020396
Lliboutry, L. (1995). Correspondence. Why calculated basal drags of ice streams can be fallacious. *Journal of Glaciology*, *41*(137), 204–205. https://doi.org/10.3189/S0022143000017901
MacGregor, K. R., Riihimaki, C. A., & Anderson, R. S. (2005). Spatial and temporal evolution of rapid basal sliding on Bench Glacier, Alaska, USA. *Journal of Glaciology*, *51*(172), 49–63. https://doi.org/10.3189/172756505781829485
Mair, D., Nienow, P., Sharp, M. J., Wohlleben, T., & Willis, I. (2002). Influence of subglacial drainage system evolution on glacier surface motion: Haut Glacier d'Arolla, Switzerland. *Journal of Geophysical Research*, *107*(B8), EPM8-1–EPM8-13. https://doi.org/10.1029/2001JB000514
Mair, D., Nienow, P., Willis, I., & Sharp, M. J. (2001). Spatial patterns of glacier motion during a high-velocity event: Haut Glacier d'Arolla, Switzerland. *Journal of Glaciology*, *47*(156), 9–20. https://doi.org/10.3189/172756501781832412
Nanni, U., Gimbert, F., Vincent, C., Gräff, D., Walter, F., Piard, L., & Moreau, L. (2020). Quantification of seasonal and diurnal dynamics of subglacial channels using seismic observations on an Alpine glacier. *The Cryosphere*, *14*(5), 1475–1496. https://doi.org/10.5194/tc-14-1475-2020
Nienow, P. W., Hubbard, A. L., Hubbard, B. P., Chandler, D. M., Mair, D. W. F., Sharp, M. J., & Willis, I. C. (2005). Hydrological controls on diurnal ice flow variability in valley glaciers. *Journal of Geophysical Research*, *110*(F4), F04002. https://doi.org/10.1029/2003JF000112
Nye, J. F. (1973). Water at the bed of a glacier. In *Proceedings of the Cambridge Symposium, 1969* (pp. 189–194). IASH.
Nye, J. F. (1976). Waterflow in glaciers: Jökulhlaups, tunnels and veins. *Journal of Glaciology*, *17*(76), 181–207. https://doi.org/10.3189/S002214300001354X
Oerlemans, J. (2001). *Glaciers and climate change*. A.A. Balkema Publishers.

Parizek, B. R., & Alley, R. B. (2004). Implications of increased Greenland surface melt under global-warming scenarios: Ice-sheet simulations. *Quaternary Science Reviews*, *23*(9–10), 1013–1027. https://doi.org/10.1016/j.quascirev.2003.12.024

Pimentel, S., & Flowers, G. E. (2010). A numerical study of hydrologically driven glacier dynamics and subglacial flooding. *Proceedings of the Royal Society London, Series A*, *467*(2126), 537–558. https://doi.org/10.1098/rspa.2010.0211

Rabatel, A., Sanchez, O., Vincent, C., & Six, D. (2018). Estimation of glacier thickness from surface mass balance and ice flow velocities: A case study on Argentière Glacier, France. *Frontiers of Earth Science*, *6*, 112. https://doi.org/10.3389/feart.2018.00112

Röthlisberger, H. (1972). Water pressure in intra- and subglacial channels. *Journal of Glaciology*, *11*(62), 177–203. https://doi.org/10.3189/S0022143000022188

Ryser, C., Lüthi, M., Andrews, C. A., Hoffman, M. J., Catania, G. A., Hawley, R. L., et al. (2014). Sustained high basal motion of the Greenland Ice Sheet revealed by borehole deformation. *Journal of Glaciology*, *60*, 222–660. https://doi.org/10.3189/2014JoG13J196

Schoof, C. (2005). The effect of cavitation on glacier sliding. *Proceedings of the Royal Society A*, *461*(2055), 609–627. https://doi.org/10.1098/rspa.2004.1350

Schoof, C. (2010). Ice-sheet acceleration driven by melt supply variability. *Nature*, *468*(7325), 803–806. https://doi.org/10.1038/nature09618

Smith, M. W., Carrivick, J. L., & Quincey, D. J. (2015). Structure from motion photogrammetry in physical geography. *Progressin Physical Geography: Earth and Environment*, *40*(2), 247–275. https://doi.org/10.1177/0309133315615805

Sole, A., Nienow, P., Bartholomew, I., Mair, D., Cowton, T., Tedstone, A., & King, M. A. (2013). Winter motion mediates dynamic response of the Greenland Ice Sheet to warmer summers. *Geophysical Research Letters*, *40*(15), 3940–3944. https://doi.org/10.1002/grl.50764

Sugiyama, S., & Gudmunsson, G. H. (2004). Short-term variations in glacier flow controlled by subglacial water pressure at Lauteraargletscher, Bernese Alps, Switzerland. *Journal of Glaciology*, *50*(170), 353–363. https://doi.org/10.3189/172756504781829846

Sundal, A. V., Shepherd, A., Nienow, P., Hanna, E., Palmer, S., & Huybrechts, P. (2011). Melt-induced speed-up of Greenland Ice Sheet offset by efficient subglacial drainage. *Nature*, *469*(7331), 521–524. https://doi.org/10.1038/nature09740

Tedstone, A. J., Nienow, P. W., Gourmelen, N., Dehecq, A., Goldberg, D., & Hanna, E. (2015). Decadal slowdown of a land-terminating sector of the Greenland Ice Sheet despite warming. *Nature*, *526*(7575), 692–695. https://doi.org/10.1038/nature15722

Thibert, E., Blanc, R., Vincent, C., & Eckert, N. (2008). Glaciological and volumetric mass balance measurements: Error analysis over 51 years for Glacier de Sarennes, French Alps. *Journal of Glaciology*, *54*(186), 522–532. https://doi.org/10.3189/002214308785837093

Thøgersen, K., Gilbert, A., Schuler, T. V., & Malthe-Sørenssen, A. (2019). Rate-and-state friction explains glacier surge propagation. *Nature Communications*, *10*(1), 2823. https://doi.org/10.1038/s41467-019-10506-4

Truffer, M., Harrison, W., & March, R. (2005). Record negative glacier balances and low velocities during the 2004 heatwave in Alaska, USA: Implications for the interpretation of observations by Zwally and others in Greenland. *Journal of Glaciology*, *51*(175), 663–664. https://doi.org/10.3189/172756505781829016

van de Wal, R. S., Boot, W., van den Broeke, M. R., Smeets, C. J., Reijmer, C. H., Donker, J. J., & Oerlemans, J. (2008). Large and rapid melt-induced velocity changes in the ablation zone of the Greenland Ice Sheet. *Science (New York, N.Y.)*, *321*(5885), 111–113. https://doi.org/10.1126/science.1158540

Vernay, M., Lafaysse, M., Monteiro, D., Hagenmuller, P., Nheili, R., Samacoïts, R., et al. (2021). The S2M meteorological and snow cover reanalysis over the French mountainous areas, description and evaluation (1958–2020). *Earth System Science Data Discussions*, 1–36. https://doi.org/10.5194/essd-021-249

Vincent, C. (2021). Ice flow velocities and uplift [Dataset]. Zenodo. https://doi.org/10.5281/zenodo.5536953

Vincent, C., Cusicanqui, D., Jourdain, B., Laarman, O., Six, D., Gilbert, A., et al. (2021). Geodetic point surface mass balances: A new approach to determine point surface mass balances on glaciers from remote sensing measurements. *The Cryosphere*, *15*(3), 1259–1276. https://doi.org/10.5194/tc-15-1259-2021

Vincent, C., & Moreau, L. (2016). Sliding velocity fluctuations and subglacial hydrology over the last two decades on Argentière Glacier, Mont Blanc area. *Journal of Glaciology*, *62*(235), 805–815. https://doi.org/10.1017/jog.2016.35

Vincent, C., Soruco, A., Six, D., & Le Meur, E. (2009). Glacier thickening and decay analysis from 50 years of glaciological observations performed on Glacier d'Argentière, Mont Blanc area, France. *Annals of Glaciology*, *50*, 73–79. https://doi.org/10.3189/172756409787769500

Vivian, R. (1975). *Les glaciers des Alpes occidentales, étude géographique* (Thesis). Institut de Géographie Alpine, University of Grenoble Alpes.

Walder, J. S. (1986). Hydraulics of subglacial cavities. *Journal of Glaciology*, *32*(112), 439–445. https://doi.org/10.3189/s0022143000012156

Walder, J. S., & Fowler, A. (1994). Channelized subglacial drainage over a deformable bed. *Journal of Glaciology*, *40*(134), 3–15. https://doi.org/10.3189/S0022143000012156

Werder, M. A., Hewitt, I. J., Schoof, C. G., & Flowers, G. E. (2013). Modeling channelized and distributed subglacial drainage in two dimensions. *Journal of Geophysical Research: Earth Surface*, *118*(4), 2140–2158. https://doi.org/10.1002/jgrf.20146

Young, T. J., Christoffersen, P., Doyle, S. H., Nicholls, K. W., Stewart, C. L., Hubbard, B., et al. (2019). Physical conditions of fast glacier flow: 3. Seasonally-evolving ice deformation on Store Glacier, West Greenland. *Journal of Geophysical Research: Earth Surface*, *124*(1), 245–267. https://doi.org/10.1029/2018JF004821

Zwally, H. J., Abdalati, W., Herring, T., Larson, K., Saba, J., & Steffen, K. (2002). Surface melt-induced acceleration of Greenland Ice-Sheet flow. *Science*, *297*(5579), 218–222. https://doi.org/10.1126/science.1072708

References From the Supporting Information

Cowton, T., Nienow, P., Sole, A., Bartholomew, I., & Mair, D. (2016). Variability in ice motion at a land-terminating Greenlandic outlet glacier: The role of channelized and distributed drainage systems. *Journal of Glaciology*, *62*(233), 451–466. https://doi.org/10.1017/jog.2016.36

Hooke, R. L. B., Brzozowski, J., & Bronge, C. (1983). Seasonal variations in surface velocity, Storglaciären, Sweden. *Geografiska Annaler – Series A: Physical Geography*, *65*(3/4), 263–277. https://doi.org/10.2307/520591

Ostling, M., & Hooke, R. L. (1986). Water Storage in Storglaciaren, Kebnekaise, Sweden. *Geografiska Annaler – Series A: Physical Geography*, *68*(4), 279–290. https://doi.org/10.2307/521521

Tangborn, W. V., Krimmel, R., & Meier, M. (1975). A comparison of glacier mass balance by glaciological, hydrological, and mapping methods, South Cascade Glacier, Washington, in General Assembly of Moscow. *IAHS Publication*, *104*, 185–196.

Willis, I. C., Sharp, M. J., & Richards, K. S. (1993). Studies of the water balance of Midtdalsbreen, Hardangerjokulen, Norway. II. Water storage and runoff prediction. *Zeitschrift für Gletscherkunde und Glazialgeologie*, *27/28*, 117–138.